

Mode-Specific Quasiclassical Dynamics of the $F^- + CH_3I$ S_N2 and Proton-Transfer Reactions

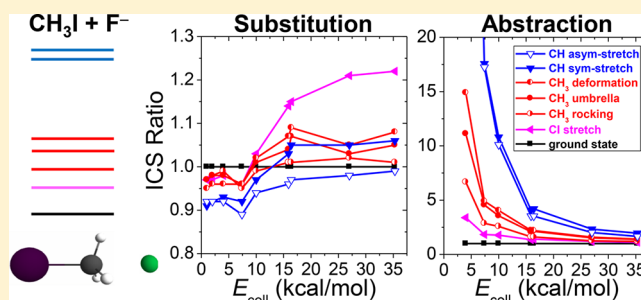
Balázs Olasz and Gábor Czakó*[✉]

Department of Physical Chemistry and Materials Science, Institute of Chemistry, University of Szeged, Rerrich Béla tér 1, Szeged H-6720, Hungary

Supporting Information

ABSTRACT: Mode-specific quasiclassical trajectory computations are performed for the $F^- + CH_3I$ ($v_k = 0, 1$) S_N2 and proton-transfer reactions at nine different collision energies in the range of 1.0–35.3 kcal/mol using a full-dimensional high-level ab initio analytical potential energy surface with ground-state and excited CI stretching (ν_3), CH_3 rocking (ν_6), CH_3 umbrella (ν_2), CH_3 deformation (ν_5), CH symmetric stretching (ν_1), and CH asymmetric stretching (ν_4) initial vibrational modes. Millions of trajectories provide statistically definitive mode-specific cross sections, opacity functions, scattering angle distributions, and product internal energy distributions.

The excitation functions reveal slight vibrational S_N2 inversion inhibition/enhancement at low/high collision energies (E_{coll}), whereas large decaying-with- E_{coll} vibrational enhancement effects for the S_N2 retention (double inversion) and proton-transfer channels. The most efficient vibrational enhancement is found by exciting the CI stretching (high E_{coll}) for S_N2 inversion and the CH stretching modes (low E_{coll}) for double inversion and proton transfer. Mode-specific effects do not show up in the scattering angle distributions and do blue-shift the hot/cold S_N2 /proton-transfer product internal energies.



I. INTRODUCTION

Selectively breaking chemical bonds and controlling reactions have always been the goal of chemists. One way to achieve this goal is provided by excitation of a specific vibrational mode of the reactant molecule, which may facilitate the cleavage of the “excited bond”, thereby increasing reactivity toward the desired products. This vibrational effect is quite obvious for reactions of diatomic molecules, especially if the transition state has a product-like structure, where the vibrational excitation helps to reach the stretched bond distance needed to go over the barrier.¹ Vibrational mode selectivity in polyatomic reactions is less understood, because polyatomic molecules have multiple vibrational modes involving concerted motions of several atoms. Excitation of those modes that couple efficiently with the reaction coordinate may promote the reaction, whereas some modes may behave as spectators and have negligible effect on the reactivity. The mode-specific dynamics of several atom plus molecule hydrogen-abstraction reactions, such as $H, F, Cl, O, Br + H_2O/HDO$ and CH_4/CHD_3 , have been extensively studied both experimentally and theoretically.^{2–18} For ion–molecule reactions, such as the $X^- + CH_3Y$ -type ($X, Y = F, Cl, Br, I, OH$, etc.) bimolecular nucleophilic substitution (S_N2), mode-specificity is less obvious, because the $X^- + CH_3Y$ systems usually have submerged barriers and support long-lived complexes in the entrance channel. Nevertheless, early experimental and theoretical studies on the $Cl^- + CH_3Cl$ and $Cl^- + CH_3Br$ S_N2 reactions found evidence for nonstatistical behavior and mode-selective vibrational enhancement of

reactivity.^{19–22} In the 2000s Hennig and Schmatz^{23–26} reported several 4-dimensional time-independent quantum dynamics studies for the above S_N2 reactions considering the vibrational effects upon CCl/CBr stretching, symmetric CH stretching, and CH_3 umbrella mode excitations. Significant vibrational enhancement was found at low collision energies, even in the case of the CH stretching excitation questioning its spectator character. For $Cl^- + CH_3I$, Kowalewski and co-workers²⁷ performed 3-dimensional time-dependent wave packet computations, where the CCl , CI , and the CH_3 umbrella modes were active. CI excitation was found to have larger effects on the reactivity than the umbrella motion. In 2016 Yang and co-workers²⁸ in collaboration with our group reported the highest-dimensional quantum dynamics study for a S_N2 reaction, namely $F^- + CH_3Cl$, using a 6-dimensional, noncollinear model and a full-dimensional high-level ab initio potential energy surface (PES).²⁹ The reduced-dimensional quantum results were found to be in good agreement with those obtained from full-dimensional quasiclassical trajectory (QCT) computations.²⁸ Later, we also performed mode-specific QCT computations for the $F^- + CHD_2Cl$ S_N2 and proton-transfer reactions.³⁰ The above studies found that CCl stretching excitation promotes the S_N2 reaction most efficiently, whereas CH excitation enhances the proton-abstraction channel.

Received: August 25, 2018

Revised: September 19, 2018

Published: September 19, 2018



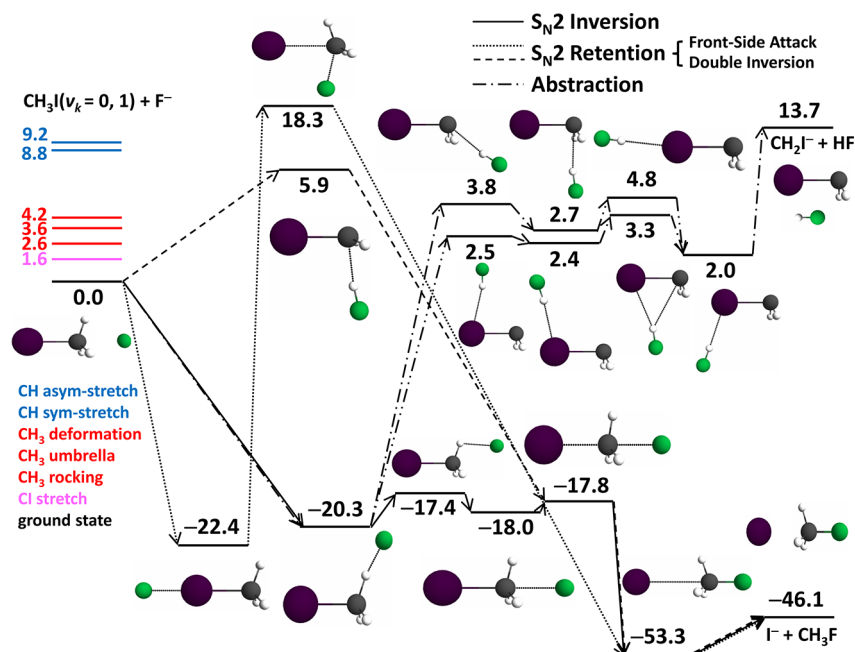


Figure 1. Schematic vibrationally adiabatic potential energy surface of the $F^- + CH_3I$ reaction showing the energies (kcal/mol) of the initial vibrational states and the stationary points relative to $F^- + CH_3I(v=0)$ corresponding to the analytical PES of ref 35.

As described above, several theoretical studies predicted various mode-specific dynamics for S_N2 reactions,¹⁹ but direct experimental study of the vibrational effects on the scattering process has been lacking until very recently. In 2018 Wester and co-workers³² measured negligible vibrational effect upon symmetric CH stretching excitation in the $F^- + CH_3I$ S_N2 reaction, thereby providing the first experimental evidence for the spectator character of this mode. To confirm the measurement of the absence of an effect, the proton-transfer product (CH_2I^-) was also detected in parallel to I^- , and unlike for the S_N2 reaction, large vibrational enhancement was observed for the proton-transfer process. These experimental findings were supported by our QCT computations and the sudden vector projection (SVP) model.³² In the above work, only the effect of the symmetric CH stretching is considered at two collision energies.³² In the present study we extend our previous work³² by performing mode-specific QCT computations for the $F^- + CH_3I$ S_N2 and proton-transfer reactions at several collision energies considering the excitation of all the six initial vibrational modes. Thus, our study may support the ongoing mode-specific experiments on the excitation of the mode(s) other than the symmetric CH stretching and reveal the collision energy dependence of the vibrational effects. A further motivation is related to a recent direct dynamics study of Hase and co-workers,³³ finding that vibrational excitations may not promote the novel double-inversion mechanism^{29,34} of the $F^- + CH_3I$ reaction. Performing the proposed computations is challenging, because double inversion has a low reaction probability and many trajectories at several initial vibrational states, impact parameters, and collision energies need to be considered to obtain reasonable statistical accuracy. The efficient QCT computations are made possible by the use of our recently developed full-dimensional high-level ab initio analytical PES,³⁵ which describes the S_N2 inversion, front-side attack and double-inversion retention pathways as well as the proton-transfer channel. In section II we give the computational details and the results are presented and discussed in section III. The paper ends with summary and conclusions in section IV.

II. COMPUTATIONAL DETAILS

Mode-specific QCT computations are performed for the $F^- + CH_3I(v_k=0, 1)$ [$k=1-6$] reactions using a full-dimensional ab initio PES taken from ref 35. The vibrational ground state ($v=0$) as well as the CI stretching ($v_3(a_1)=1$), CH_3 rocking ($v_6(e)=1$), CH_3 umbrella ($v_2(a_1)=1$), CH_3 deformation ($v_5(e)=1$), CH symmetric stretching ($v_1(a_1)=1$), and CH asymmetric stretching ($v_4(e)=1$) states, excited by one quantum, are prepared using normal mode sampling.³⁶ (Note that the excited reactant usually maintains its mode-specific character prior to interaction as seen for CHD_2Cl in ref 30.) Trajectories are run at collision energies (E_{coll}) of 1.0, 2.0, 4.0, 7.4, 10.0, 15.9, 16.4, 27.0, and 35.3 kcal/mol using 0.0726 fs time steps until the longest interatomic separation becomes 1 bohr larger than the initial one. Some of the collision energies are selected to match previous experimental values.^{32,37} The initial orientation of the reactants is randomly sampled and their distance is set to $(x^2 + b^2)^{1/2}$, where b is the impact parameter and x is 40 bohr at $E_{coll}=1.0$ kcal/mol, 30 bohr at $E_{coll}=2.0$ and 4.0 kcal/mol, and 20 bohr at the larger E_{coll} . The impact parameter is scanned from 0 to b_{max} with step size of 0.5 bohr and the maximum impact parameters (b_{max}) vary between 11 and 30 bohr depending strongly on E_{coll} and slightly on the initial vibrational state. A total of 5000 trajectories are computed at each b , which results in millions of trajectories considering that we have 7 initial vibrational states and 9 different collision energies. The mode-specific integral and differential cross sections are obtained by a b -weighted numerical integration of the reaction probabilities over impact parameters. Differential cross sections are obtained without zero-point energy (ZPE) constraint, whereas for the integral cross sections of the proton-transfer reaction soft and hard ZPE constraints are also applied. Note that ZPE violation is found negligible for the S_N2 channel, as expected for a highly exothermic reaction. Soft constraint means discarding trajectories if the sum of the product vibrational energies is less than the sum of the corresponding ZPEs. Hard constraint discards trajectories if either product violates ZPE.

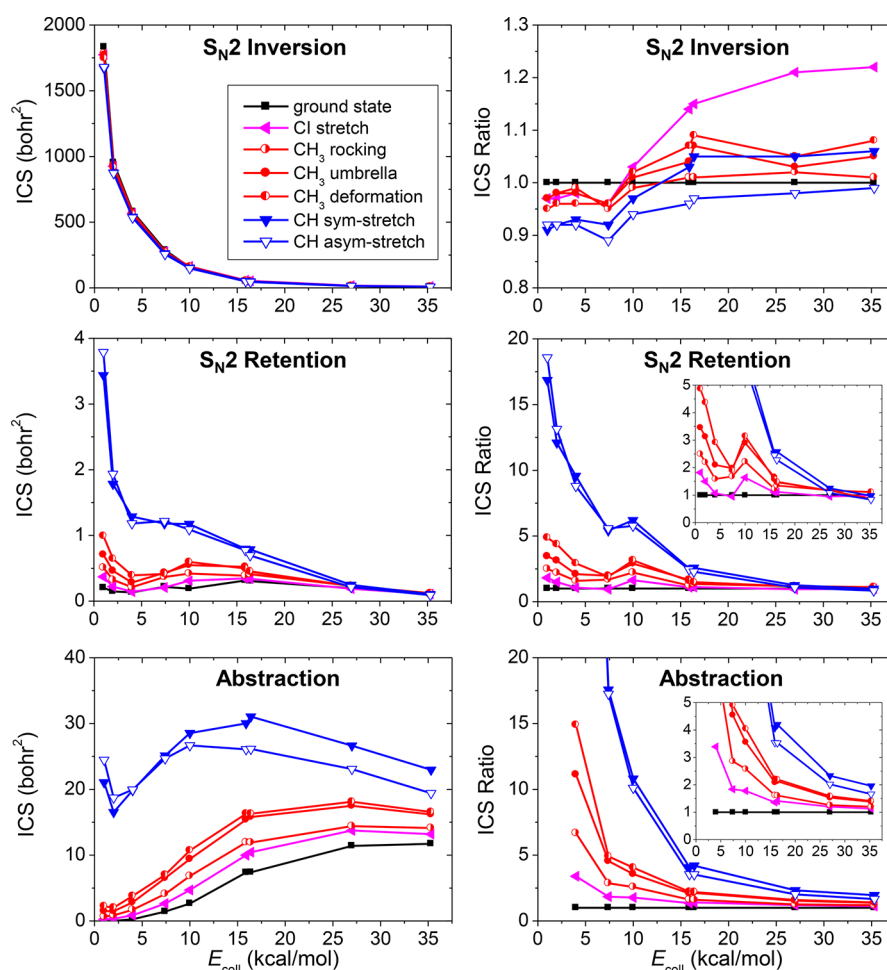


Figure 2. Mode-specific cross sections and $(\nu_k = 1)/(\nu_k = 0)$ cross section ratios as a function of collision energy for the S_N2 inversion, S_N2 retention, and abstraction channels of the $F^- + CH_3I(\nu_k = 0, 1)$ reactions.

III. RESULTS AND DISCUSSION

The $F^- + CH_3I$ reaction can proceed with different mechanisms as shown in Figure 1. The S_N2 products ($I^- + CH_3F$, $\Delta H_0 = -46.1$ kcal/mol on the PES) can be formed with Walden inversion via several submerged complexes and transition states. Furthermore, S_N2 reaction can occur with retention of configuration via the front-side attack and the double-inversion pathways. The former has a high adiabatic barrier of 18.3 kcal/mol, whereas double inversion can proceed, without following an intrinsic reaction coordinate,³³ via a transition state only 5.9 kcal/mol above the reactants. Besides the highly exothermic S_N2 channel, proton transfer forming $HF + CH_2I^-$ can occur via several stationary points below the product asymptote ($\Delta H_0 = 13.7$ kcal/mol).^{35,38} Note that the double-inversion barrier height is below the energy level of the $HF + CH_2I^-$ products; thus, double inversion may occur at collision energies below the proton-transfer threshold.

Mode-specific integral cross sections and vibrational enhancement factors as a function of E_{coll} are shown in Figure 2. The S_N2 inversion cross sections are extremely large at low collision energies and decrease as E_{coll} increases, as expected in the case of a highly exothermic barrierless reaction. At low E_{coll} up to about 10 kcal/mol reactant vibrational excitation hinders the reaction by about 10% for the CH stretching excitation and by 3–5% for the other modes. At larger collision energies, for example, in the 15–35 kcal/mol range, symmetric CH stretching excitation

increases the reactivity, relative to the ground-state reaction, by 5–6%, whereas asymmetric CH excitation shows a few % inhibition effect (Figure 2). CH_3 rocking motion has negligible effect on the reactivity (<1–2%), umbrella excitation increases the cross sections by about 5%, and CH_3 deformation has about 8% enhancement effect. The largest enhancement of about 20% (increasing from 14 to 22% in the E_{coll} range of 15.9–35.3 kcal/mol) is found upon CI stretching excitation. The fact that CI stretching excitation is the most efficient to promote the S_N2 channel is expected, because the CI bond breaks in this process. This finding is also in accord with the large SVP value of the CI mode corresponding to the Walden-inversion transition state.³² The SVP model³⁹ and chemical intuition suggest that the second most efficient mode should be the CH_3 umbrella, whose excitation may facilitate inversion of the methyl group. Umbrella excitation indeed promotes the reaction at large E_{coll} , but unexpectedly CH_3 deformation has somewhat larger enhancement effect in disagreement with the SVP prediction. Note that the SVP model is only valid for the direct reaction, where vibration energy redistribution is negligible in the entrance channel. For the title reaction indirect mechanisms are significant,^{40,35,41} which may compromise some of the SVP predictions.

One can compare the present results to those obtained for the seemingly similar $F^- + CH_3Cl$ S_N2 reaction, although for the $F^- + CH_3Cl$ reaction mode-specific cross sections were reported only in the E_{coll} range of 1–10 kcal/mol (Figure S3 of ref 28). Interestingly, in most cases, except for some of the modes in the

1–4 kcal/mol E_{coll} range, vibrational enhancement was found in $\text{F}^- + \text{CH}_3\text{Cl}$, whereas inhibition is seen for the $\text{F}^- + \text{CH}_3\text{I}$ reaction. For example, about 10–40% enhancement was found upon CCl stretching excitation in the 1–10 kcal/mol E_{coll} range,²⁸ whereas CI excitation has a 2–3% hindering effect in the same E_{coll} range. The reason for this difference may be due to the fact that the $\text{F}^- + \text{CH}_3\text{Cl}$ reaction is more direct, i.e., direct mechanisms dominate in $\text{F}^- + \text{CH}_3\text{Cl}$, whereas $\text{F}^- + \text{CH}_3\text{I}$ mainly proceeds via indirect, complex-forming pathways,⁴⁰ thereby $\text{F}^- + \text{CH}_3\text{Cl}$ shows more pronounced vibrational enhancement effects.

Mode-specific $\text{S}_{\text{N}}2$ retention cross sections via the front-side attack and double-inversion pathways are also shown in Figure 2. Note that whereas for $\text{F}^- + \text{CH}_3\text{Cl}$ we found that one can distinguish between front-side attack and double inversion on the basis of the integration time,²⁹ we find this approach not definitive for the $\text{F}^- + \text{CH}_3\text{I}$ reaction; therefore, we give the total retention cross sections. Nevertheless, trajectory animations show that at low E_{coll} double inversion dominates the retention process, as expected based on its significantly lower barrier (5.9 vs 18.3 kcal/mol). Retention cross sections are about 2 orders of magnitude lower than the inversion ones and show significant mode-specificity, especially at low collision energies. For the $\text{F}^- + \text{CH}_3\text{I}(\nu = 0)$ reaction the cross sections are around 0.1–0.3 bohr,² and they increase by a factor of 1–2 upon CI stretching, 2–5 upon CH_3 bending, and 5–20 upon CH stretching excitations. These enhancement factors have strong E_{coll} dependence; the vibrational effects are the largest at low E_{coll} and diminish at around 27 kcal/mol. The finding that symmetric/asymmetric CH stretching excitations substantially enhance double inversion, for example, by factors of 17/19, 12/13, 10/9, 5/6, and 6/6 at E_{coll} of 1.0, 2.0, 4.0, 7.4, and 10.0 kcal/mol, respectively, can be explained by the fact that CH excitations help to access the $\text{FH}\cdots\text{CH}_2\text{I}^-$ -type double-inversion transition state. In other words, the first step of double inversion is a proton-abstraction-induced inversion which is facilitated by exciting the CH stretching mode(s). As mentioned in the Introduction, Hase and co-workers³³ performed direct dynamics simulations considering the effects of the CH_3 deformation and the CH stretching modes. 200 trajectories were run for each initial states (combination bands excited by 1 quantum or 2 quanta in each mode) at $b = 0$ and $E_{\text{coll}} = 10$ and 20 kcal/mol. A total of 1–3 double inversion trajectories were found, which corresponds to reaction probabilities of 0.5–1.5%. The authors correctly concluded that these reaction probabilities are small; however, possible vibrational enhancement could not be determined, because trajectories were not run for ground-state CH_3I . Therefore, we cannot fully agree with their statement that the “ $\text{S}_{\text{N}}2$ double inversion is not highly promoted”³³ upon vibrational excitation and we have done further investigations with the following results: On one hand, at $E_{\text{coll}} = 10$ kcal/mol, our computations give 50 and 74/91 retention trajectories from 5000 for the CH_3 deformation and symmetric/asymmetric CH stretching excited reactants, respectively, corresponding to reaction probabilities of 1.0 and 1.5/1.8%, in agreement with the direct dynamics results. On the other hand, we obtained only 18 retention trajectories (0.4%) for the ground-state reaction, showing significant vibrational enhancement effects. Furthermore, considering our mode-specific cross sections at $E_{\text{coll}} = 10$ kcal/mol, vibrational enhancements by factors of 3, 6, and 6 upon one quantum excitation of the CH_3 deformation, symmetric CH stretching, and asymmetric CH stretching modes are obtained, respectively. We do not have results at $E_{\text{coll}} = 20$ kcal/mol,

nevertheless, at $E_{\text{coll}} = 16.4$ kcal/mol the above factors are 1.5, 2.6, and 2.3 and at $E_{\text{coll}} = 27$ kcal/mol the factors are 1.2, 1.3, and 1.1. As seen, at large E_{coll} the vibrational enhancement diminishes, as mentioned above, however, at low E_{coll} , for example at 10 kcal/mol, substantial enhancement is found, especially upon CH stretching excitation.

Proton abstraction (proton transfer from CH_3I to F^-) cross sections of the $\text{F}^- + \text{CH}_3\text{I}(\nu = 0)$ reaction increase with collision energy. At low E_{coll} , the endothermic proton abstraction is basically closed and at larger E_{coll} around 30 kcal/mol abstraction cross sections have similar magnitude as $\text{S}_{\text{N}}2$ ones. Initial vibrational excitations enhance the proton-abstraction channel and the enhancement effects decrease with increasing E_{coll} . Similar to the $\text{S}_{\text{N}}2$ retention pathways, the enhancement factors increase as CI stretching, CH_3 bending, and CH stretching. At low E_{coll} , the CH stretching excitation opens the abstraction channel, and the vibrational enhancement factors are around 78, 17, 10, 4, and 2 at $E_{\text{coll}} = 4.0, 7.4, 10.0, 16.4,$ and 35.3 kcal/mol, respectively. At larger E_{coll} symmetric CH stretching excitation promotes the proton transfer more efficiently than the asymmetric CH stretching mode (Figure 2), despite the fact that the former has slightly less energy. These large symmetric CH stretching enhancement effects on the reactivity of the proton-transfer channel are in agreement with the recent crossed-beam experiment of Wester and co-workers.³²

For the endothermic proton-abstraction channel one may expect significant product ZPE violation; thus, we have considered different ZPE constrained analysis techniques. The mode-specific excitation functions for the abstraction channel obtained without ZPE constraint are compared with soft and hard constrained results in Figure 3. ZPE constraint reduces the cross sections and shifts the threshold energies toward larger collision energies. Without ZPE constraint, small nonzero $\text{F}^- + \text{CH}_3\text{I}(\nu = 0)$ abstraction cross sections are obtained at E_{coll} values below the endothermicity of 13.7 kcal/mol. These unphysical cross sections, due to the classical nature of the QCT calculations, vanish and the threshold shifts to about 15 kcal/mol even with the soft constraint. Reactant vibrational excitation increases the cross sections and allows opening the abstraction pathways at lower collision energies. However, unlike in the unconstrained case, even for the CH stretching-excited reaction threshold energy of about 7 kcal/mol still exists. The relative efficiency of the different vibrational modes in the enhancement of the proton-abstraction reaction is similar with and without ZPE constraint.

Mode-specific opacity functions (reaction probabilities as a function of b) as well as scattering angle and product internal energy distributions are given in Figures 4 and 5 for the $\text{S}_{\text{N}}2$ and proton-transfer channels, respectively. These results are presented at four representative collision energies of 1.0, 7.4, 16.4, and 27.0 kcal/mol, while a more complete picture showing all the results at nine different E_{coll} in the 1.0–35.3 kcal/mol range is presented in the Supporting Information (Figures S1–S3). As Figure 4 shows $\text{S}_{\text{N}}2$ reaction probabilities are large and decrease with increasing E_{coll} . At $E_{\text{coll}} = 1.0$ kcal/mol, the opacity function is broad, showing a nearly constant reaction probability around 80–90% up to $b = 15$ bohr, where the opacity function starts to decay and finally drops to zero between $b = 25$ and 30 bohr. At larger E_{coll} , the b_{max} value becomes smaller and smaller and the opacity function decreases almost linearly between $b = 0$ and b_{max} . The shape of the opacity functions is determined by long-range ion-dipole interactions, which facilitate reaction at large impact parameters, especially at low collision energies.

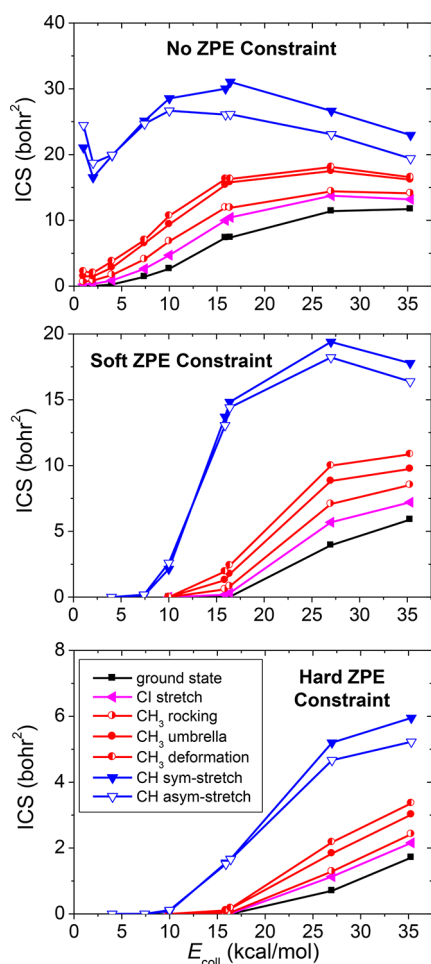


Figure 3. Mode-specific cross sections as a function of collision energy for the $F^- + CH_3I(v_k = 0, 1) \rightarrow HF + CH_2I^-$ reactions obtained without ZPE constraint as well as with soft, discarding trajectories if $E_{vib}(HF) + E_{vib}(CH_2I^-) < ZPE(HF) + ZPE(CH_2I^-)$, and hard, discarding trajectories if $E_{vib}(HF) < ZPE(HF)$ or $E_{vib}(CH_2I^-) < ZPE(CH_2I^-)$ ZPE constraints.

Significant mode-specificity is not seen in the S_N2 reaction probability functions. The picture is different in the case of the proton-transfer channel. As Figure 5 shows vibrational excitations substantially increase the abstraction probabilities, especially in the case of CH stretching excitations. At $E_{coll} = 1.0$ kcal/mol virtually no reactivity is seen for the ground-state reaction, whereas the reaction probability becomes 1–2% upon CH stretching excitation. At $E_{coll} = 7.4, 16.4,$ and 27.0 kcal/mol, the $b = 0$ abstraction probabilities are 0.4, 3.6, and 7.0%, respectively, for the $F^- + CH_3I(v = 0)$ reaction, whereas the corresponding values are 5.3/5.5, 12.3/11.3, and 12.1/11.0% for the symmetric/asymmetric CH stretching-excited reactions. The b_{max} values of the S_N2 and proton-transfer reactions are very similar, indicating that the long-range prereaction interactions determine the maximum impact parameters.

Scattering angle distributions of both the S_N2 and proton-transfer reactions show almost no mode-specificity, in accord with the similar shape of the opacity functions corresponding to different reactant vibrational states (Figures 4 and 5). The S_N2 reaction features very isotropic angular distributions, with forward preference at low E_{coll} . As E_{coll} increases this forward preference diminishes and slight backward dominance appears at $E_{coll} = 35.3$ kcal/mol (Figure S2) indicating the increased

probability of the direct reaction. The abstraction scattering distributions are nearly backward-forward symmetric at low collision energies, and become forward scattered as E_{coll} increases, for example, at $E_{coll} = 27.0$ kcal/mol (Figure 5), in good agreement with the CH stretching-excited experimental data.³² The dominance of forward scattering indicates that stripping mechanism plays an important role in the proton-transfer process at large E_{coll} .

Product internal energy distributions are hot for the S_N2 channel peaking at the highest available internal energies, especially at low E_{coll} , showing that the title reaction is predominantly indirect (Figure 4). As E_{coll} increases the distributions become broader and broader and the maximum internal energy shifts with the amount of E_{coll} . Here mode specificity can be observed, because the distributions shift toward larger energies and the shifting is virtually the same as the initial vibrational excitation energy. Thus, the CH_3F internal energy distributions indicate that the reactant vibrational energy mainly transfers to the product molecule. Unlike the S_N2 product internal energy distributions, the CH_2I^- distributions are Gaussian-like and cold, with many product molecules violating ZPE; see the negative part of the internal energy distributions in Figure 5. At $E_{coll} = 1.0$ kcal/mol, all the product molecules, except a small fraction from the CH stretching-excited reactions, have less internal energy than the ZPE of CH_2I^- . As E_{coll} increases the distributions shift toward higher internal energies and, thus, ZPE violation becomes less significant. At $E_{coll} = 27.0$ kcal/mol, most of the product molecules have at least ZPE even in the case of the ground-state reaction. These findings are in accord with the ZPE-constrained abstraction cross sections shown in Figure 3.

IV. SUMMARY AND CONCLUSIONS

There has recently been a renewed interest in studying mode specificity in S_N2 reactions,^{27–33} thereby extending our current knowledge on mode-specific chemical reactivity mainly accumulated by investigating atom plus molecule reactions. Experimentally, Wester and co-workers have been recently doing pioneering work by imaging S_N2 and proton-transfer reactions with infrared-excited reactants using the crossed-beam technique.³² Theoretically, our new high-level ab initio analytical PESs^{29,35,42,43} open the door for efficient quasiclassical as well as quantum simulations²⁸ of S_N2 reactions, which motivates others to study these systems with direct dynamics^{33,38} or with quantum mechanical/molecular mechanics method.^{44,45}

In the present work, we report a detailed QCT study of the mode-specific dynamics of the $F^- + CH_3I$ reaction considering excitations of all the fundamental initial vibrational modes at nine different collision energies, thereby extending our joint experimental–theoretical work³² that investigated the symmetric CH stretching effects at two collision energies. We find that at low E_{coll} below 10 kcal/mol, all the vibrational mode excitations hinder the S_N2 reaction, whereas at larger E_{coll} , most of the vibrational excitations, except the asymmetric CH stretching mode, slightly enhance the S_N2 reaction usually with a few % cross section increase. The most efficient mode is the CI stretching, causing 10–20% enhancement depending on E_{coll} . The S_N2 retention channel is substantially enhanced upon CH stretching excitations, especially at low E_{coll} , where enhancement factors over 10 can be obtained. The bending modes, most efficiently the CH_3 deformation, can also promote S_N2 retention, most likely double inversion, by factors of 2–5 in

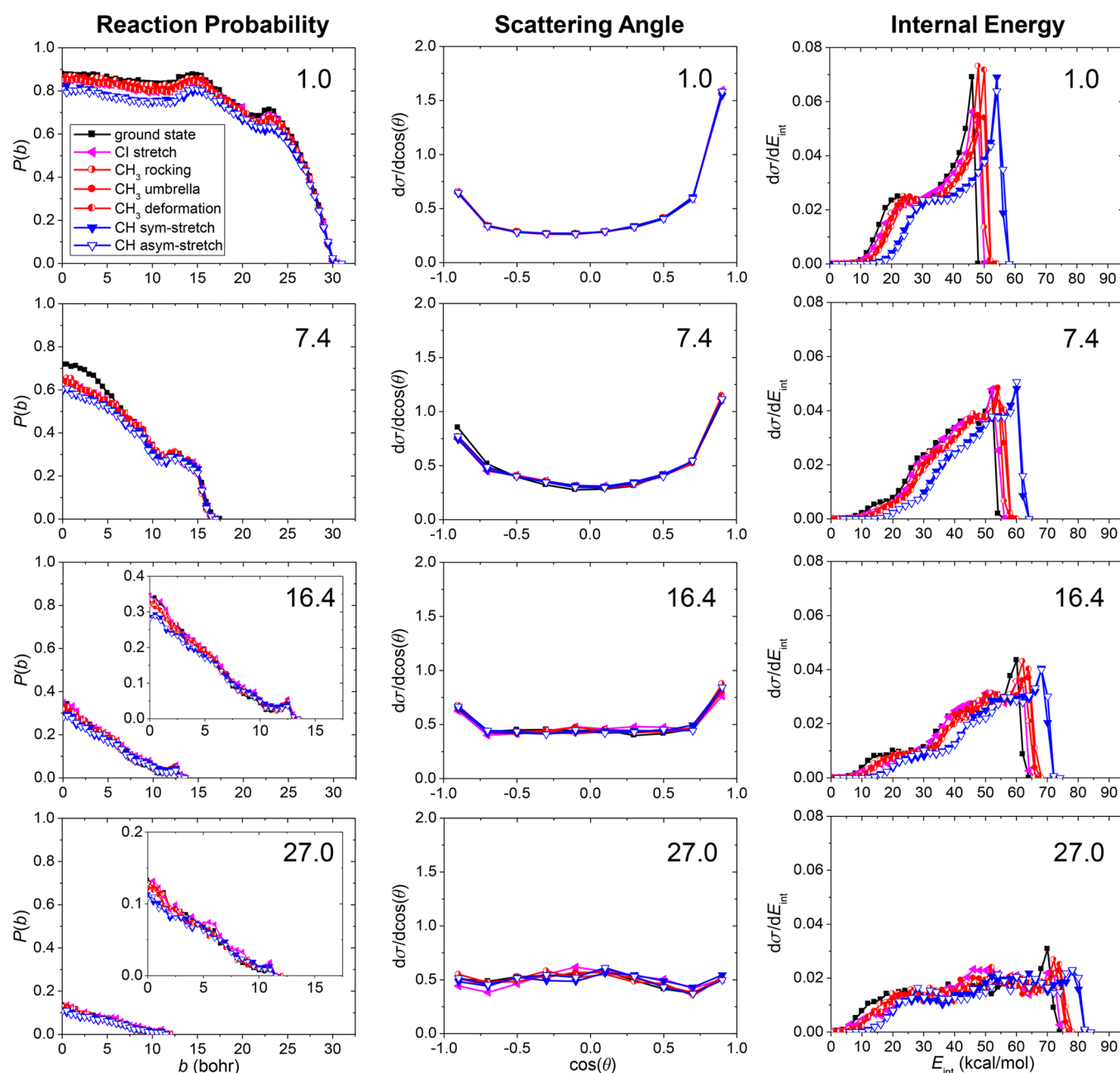
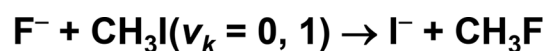


Figure 4. Mode-specific opacity functions, normalized scattering angle distributions, and normalized product internal energy, relative to the ZPE of CH_3F , distributions for the $\text{F}^- + \text{CH}_3\text{I}(v_k = 0, 1) \rightarrow \text{I}^- + \text{CH}_3\text{F}$ $\text{S}_{\text{N}}2$ reactions at collision energies of 1.0, 7.4, 16.4, and 27.0 kcal/mol. Note that the scattering angle distributions, especially at $E_{\text{coll}} = 1.0$ kcal/mol, virtually overlap.

the E_{coll} range of 1–10 kcal/mol. Therefore, in disagreement with previous work,³³ we find that vibrational excitation is a promising way to facilitate the novel double-inversion pathway^{29,31} in $\text{S}_{\text{N}}2$ reactions. Similar to the $\text{S}_{\text{N}}2$ retention channel, proton transfer also shows significant mode specificity. CH stretching excitations substantially enhance the reactivity with extremely large enhancement factors at low E_{coll} (threshold effect) and by factors of about 10 and 2 at $E_{\text{coll}} = 10$ and 35 kcal/mol, respectively. The $\text{S}_{\text{N}}2$ and proton-transfer scattering angle distributions show virtually no mode specificity, in accord with the similar shape of the mode-specific opacity functions. Product internal energy distributions are hot and cold for the $\text{S}_{\text{N}}2$ and

proton-abstraction processes, respectively, shifting toward higher internal energies with increasing reactant vibrational excitation and collision energy.

As our results demonstrate, mode-specific effects can occur in barrier-less exothermic $\text{S}_{\text{N}}2$ reactions. Furthermore, initial vibrational excitation may help to promote proton transfer or proton-abstraction-induced processes, like double inversion, in ion–molecule reactions. As internal energy redistribution may be significant in this indirect reaction studied in this work, quantum dynamical calculations, at least in reduced dimensions and perhaps using our analytical PES, would be desired in the near future. Furthermore, the present theoretical results may

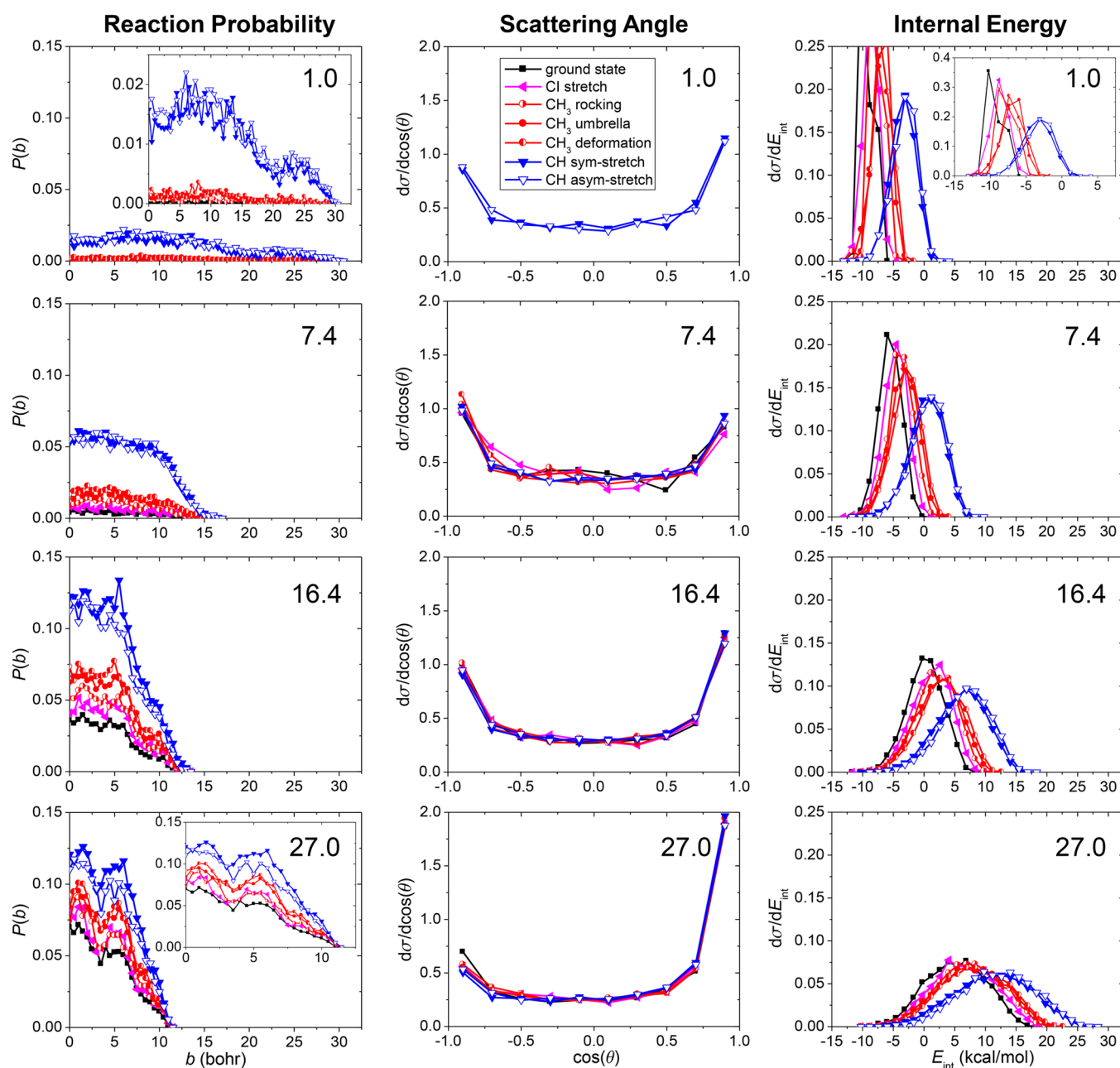


Figure 5. Mode-specific opacity functions, normalized scattering angle distributions, and normalized CH_2I^- product internal energy, relative to the ZPE of CH_2I^- , distributions for the $\text{F}^- + \text{CH}_3\text{I}(\nu_k = 0, 1) \rightarrow \text{HF} + \text{CH}_2\text{I}^-$ proton-transfer reactions at collision energies of 1.0, 7.4, 16.4, and 27.0 kcal/mol. Note that the scattering angle distributions at $E_{\text{coll}} = 1.0$ kcal/mol are only shown for the CH stretching modes, because the statistical uncertainty is too large for the other modes.

help ongoing mode-specific experiments and motivate future studies to investigate reactant vibrational effects in ion–molecule reactions.

■ ASSOCIATED CONTENT

Supporting Information

The Supporting Information is available free of charge on the ACS Publications website at DOI: 10.1021/acs.jpca.8b08286.

Mode-specific opacity functions, scattering angle distributions, and product internal energy distributions for the $\text{F}^- + \text{CH}_3\text{I}$ $\text{S}_{\text{N}}2$ and proton-transfer reactions at nine

different collision energies in the range 1.0–35.3 kcal/mol (PDF)

■ AUTHOR INFORMATION

Corresponding Author

*(G.C.) E-mail: gczako@chem.u-szeged.hu.

ORCID

Gábor Czakó: 0000-0001-5136-4777

Notes

The authors declare no competing financial interest.

ACKNOWLEDGMENTS

This work was supported by the National Research, Development and Innovation Office—NKFIH, K-125317. We thank the National Information Infrastructure Development Institute for awarding us access to resources based in Hungary at Szeged and Debrecen.

REFERENCES

- (1) Polanyi, J. C. Some Concepts in Reaction Dynamics. *Science* **1987**, *236*, 680–690.
- (2) Schatz, G. C.; Colton, M. C.; Grant, J. L. A Quasiclassical Trajectory Study of the State-to-State Dynamics of $\text{H} + \text{H}_2\text{O} \rightarrow \text{OH} + \text{H}_2$. *J. Phys. Chem.* **1984**, *88*, 2971–2977.
- (3) Sinha, A.; Hsiao, M. C.; Crim, F. F. Bond-Selected Bimolecular Chemistry: $\text{H} + \text{HOD}(4\nu_{\text{OH}}) \rightarrow \text{OD} + \text{H}_2$. *J. Chem. Phys.* **1990**, *92*, 6333–6335.
- (4) Bronikowski, M. J.; Simpson, W. R.; Girard, B.; Zare, R. N. Bond-Specific Chemistry: OD:OH Product Ratios for the Reactions $\text{H} + \text{HOD}(100)$ and $\text{H} + \text{HOD}(001)$. *J. Chem. Phys.* **1991**, *95*, 8647–8648.
- (5) Zhang, D. H.; Light, J. C. Mode Specificity in the $\text{H} + \text{HOD}$ Reaction. Full-Dimensional Quantum Study. *J. Chem. Soc., Faraday Trans.* **1997**, *93*, 691–697.
- (6) Yan, S.; Wu, Y. T.; Zhang, B.; Yue, X.-F.; Liu, K. Do Vibrational Excitations of CHD_3 Preferentially Promote Reactivity Toward the Chlorine Atom? *Science* **2007**, *316*, 1723–1726.
- (7) Zhang, W.; Kawamata, H.; Liu, K. CH Stretching Excitation in the Early Barrier $\text{F} + \text{CHD}_3$ Reaction Inhibits CH Bond Cleavage. *Science* **2009**, *325*, 303–306.
- (8) Czakó, G.; Bowman, J. M. Quasiclassical Trajectory Calculations of Correlated Product Distributions for the $\text{F} + \text{CHD}_3(v_1 = 0, 1)$ Reactions Using an Ab Initio Potential Energy Surface. *J. Chem. Phys.* **2009**, *131*, 244302.
- (9) Czakó, G.; Bowman, J. M. Dynamics of the Reaction of Methane with Chlorine Atom on an Accurate Potential Energy Surface. *Science* **2011**, *334*, 343–346.
- (10) Czakó, G. Accurate Ab Initio Potential Energy Surface, Thermochemistry, and Dynamics of the $\text{Br}(^2\text{P}, ^2\text{P}_{3/2}) + \text{CH}_4 \rightarrow \text{HBr} + \text{CH}_3$ Reaction. *J. Chem. Phys.* **2013**, *138*, 134301.
- (11) Meng, F.; Yan, W.; Wang, D. Y. Quantum Dynamics Study of the $\text{Cl} + \text{CH}_4 \rightarrow \text{HCl} + \text{CH}_3$ Reaction: Reactive Resonance, Vibrational Excitation Reactivity, and Rate Constants. *Phys. Chem. Chem. Phys.* **2012**, *14*, 13656–13662.
- (12) Czakó, G.; Bowman, J. M. Reaction Dynamics of Methane with F, O, Cl, and Br on ab Initio Potential Energy Surfaces. *J. Phys. Chem. A* **2014**, *118*, 2839–2864.
- (13) Espinosa-García, J. Role of the C–H Stretch Mode Excitation in the Dynamics of the $\text{Cl} + \text{CHD}_3$ Reaction: A Quasi-Classical Trajectory Calculation. *J. Phys. Chem. A* **2007**, *111*, 9654–9661.
- (14) Song, H.; Guo, H. Vibrational and Rotational Mode Specificity in the $\text{Cl} + \text{H}_2\text{O} \rightarrow \text{HCl} + \text{OH}$ Reaction: A Quantum Dynamical Study. *J. Phys. Chem. A* **2015**, *119*, 6188–6194.
- (15) Xie, C.; Jiang, B.; Yang, M.; Guo, H. State-to-State Mode Specificity in $\text{F} + \text{CHD}_3 \rightarrow \text{HF}/\text{DF} + \text{CD}_3/\text{CHD}_2$ Reaction. *J. Phys. Chem. A* **2016**, *120*, 6521–6528.
- (16) Welsch, R.; Manthe, U. Full-Dimensional and Reduced-Dimensional Calculations of Initial State-Selected Reaction Probabilities Studying the $\text{H} + \text{CH}_4 \rightarrow \text{H}_2 + \text{CH}_3$ Reaction on a Neural Network PES. *J. Chem. Phys.* **2015**, *142*, 064309.
- (17) Qi, J.; Song, H.; Yang, M.; Palma, J.; Manthe, U.; Guo, H. Communication: Mode Specific Quantum Dynamics of the $\text{F} + \text{CHD}_3 \rightarrow \text{HF} + \text{CD}_3$ Reaction. *J. Chem. Phys.* **2016**, *144*, 171101.
- (18) Chen, J.; Xu, X.; Liu, S.; Zhang, D. H. A Neural Network Potential Energy Surface for the $\text{F} + \text{CH}_4$ Reaction Including Multiple Channels Based on Coupled Cluster Theory. *Phys. Chem. Chem. Phys.* **2018**, *20*, 9090–9100.
- (19) Vande Linde, S. R.; Hase, W. L. A Direct Mechanism for $\text{S}_{\text{N}}2$ Nucleophilic Substitution Enhanced by Mode Selective Vibrational Excitation. *J. Am. Chem. Soc.* **1989**, *111*, 2349–2351.
- (20) Viggiano, A. A.; Morris, R. A.; Paschkewitz, J. S.; Paulson, J. F. Kinetics of the Gas-Phase Reactions of Cl^- with CH_3Br and CD_3Br : Experimental Evidence for Nonstatistical Behavior? *J. Am. Chem. Soc.* **1992**, *114*, 10477–10482.
- (21) Ayotte, P.; Kim, J.; Kelley, J. A.; Nielsen, S. B.; Johnson, M. A. Photoactivation of the $\text{Cl}^- + \text{CH}_3\text{Br}$ $\text{S}_{\text{N}}2$ Reaction via Rotationally Resolved C–H Stretch Excitation of the $\text{Cl}^- \cdot \text{CH}_3\text{Br}$ Entrance Channel Complex. *J. Am. Chem. Soc.* **1999**, *121*, 6950–6951.
- (22) Tonner, D. S.; McMahon, T. B. Non-Statistical Effects in the Gas Phase $\text{S}_{\text{N}}2$ Reaction. *J. Am. Chem. Soc.* **2000**, *122*, 8783–8784.
- (23) Hennig, C.; Schmatz, S. State-Selected Dynamics of the Complex-Forming Bimolecular Reaction $\text{Cl}^- + \text{CH}_3\text{Cl} \rightarrow \text{ClCH}_3 + \text{Cl}^-$: A Four-Dimensional Quantum Scattering Study. *J. Chem. Phys.* **2004**, *121*, 220–236.
- (24) Schmatz, S. Quantum Dynamics of Gas-Phase $\text{S}_{\text{N}}2$ Reactions. *ChemPhysChem* **2004**, *5*, 600–617.
- (25) Hennig, C.; Schmatz, S. Four-Dimensional Quantum Study on Exothermic Complex-Forming Reactions: $\text{Cl}^- + \text{CH}_3\text{Br} \rightarrow \text{ClCH}_3 + \text{Br}^-$. *J. Chem. Phys.* **2005**, *122*, 234307.
- (26) Hennig, C.; Schmatz, S. Spectator Modes in Reaction Dynamics Revisited: Reaction Cross Sections and Rate Constant for $\text{Cl}^- + \text{CH}_3\text{Br} \rightarrow \text{ClCH}_3 + \text{Br}^-$ from Quantum Scattering. *Chem. Phys. Lett.* **2007**, *446*, 250–255.
- (27) Kowalewski, M.; Mikosch, J.; Wester, R.; de Vivie-Riedle, R. Nucleophilic Substitution Dynamics: Comparing Wave Packet Calculations with Experiment. *J. Phys. Chem. A* **2014**, *118*, 4661–4669.
- (28) Wang, Y.; Song, H.; Szabó, I.; Czakó, G.; Guo, H.; Yang, M. Mode-Specific $\text{S}_{\text{N}}2$ Reaction Dynamics. *J. Phys. Chem. Lett.* **2016**, *7*, 3322–3327.
- (29) Szabó, I.; Czakó, G. Revealing a Double-Inversion Mechanism for the $\text{F}^- + \text{CH}_3\text{Cl}$ $\text{S}_{\text{N}}2$ Reaction. *Nat. Commun.* **2015**, *6*, 5972.
- (30) Szabó, I.; Czakó, G. Mode-Specific Multi-Channel Dynamics of the $\text{F}^- + \text{CHD}_2\text{Cl}$ Reaction on a Global ab Initio Potential Energy Surface. *J. Chem. Phys.* **2016**, *145*, 134303.
- (31) Szabó, I.; Czakó, G. Dynamics and Novel Mechanisms of $\text{S}_{\text{N}}2$ Reactions on ab Initio Analytical Potential Energy Surfaces. *J. Phys. Chem. A* **2017**, *121*, 9005–9019.
- (32) Stei, M.; Carrascosa, E.; Dörfler, A.; Meyer, J.; Olasz, B.; Czakó, G.; Li, A.; Guo, H.; Wester, R. Stretching Vibration Is Spectator in Nucleophilic Substitution. *Sci. Adv.* **2018**, *4*, eaas9544.
- (33) Ma, Y.-T.; Ma, X.; Li, A.; Guo, H.; Yang, L.; Zhang, J.; Hase, W. L. Potential Energy Surface Stationary Points and Dynamics of the $\text{F}^- + \text{CH}_3\text{I}$ Double Inversion Mechanism. *Phys. Chem. Chem. Phys.* **2017**, *19*, 20127–20136.
- (34) Szabó, I.; Czakó, G. Double-Inversion Mechanisms of the $\text{X}^- + \text{CH}_3\text{Y}$ [$\text{X}, \text{Y} = \text{F}, \text{Cl}, \text{Br}, \text{I}$] $\text{S}_{\text{N}}2$ Reactions. *J. Phys. Chem. A* **2015**, *119*, 3134–3140.
- (35) Olasz, B.; Szabó, I.; Czakó, G. High-Level ab Initio Potential Energy Surface and Dynamics of the $\text{F}^- + \text{CH}_3\text{I}$ $\text{S}_{\text{N}}2$ and Proton-Transfer Reactions. *Chem. Sci.* **2017**, *8*, 3164–3170.
- (36) Hase, W. L. *Encyclopedia of Computational Chemistry*; Wiley: New York, 1998; pp 399–407.
- (37) Mikosch, J.; Zhang, J.; Trippel, S.; Eichhorn, C.; Otto, R.; Sun, R.; de Jong, W. A.; Weidemüller, M.; Hase, W. L.; Wester, R. Indirect Dynamics in a Highly Exoergic Substitution Reaction. *J. Am. Chem. Soc.* **2013**, *135*, 4250–4259.
- (38) Zhang, J.; Xie, J.; Hase, W. L. Dynamics of the $\text{F}^- + \text{CH}_3\text{I} \rightarrow \text{HF} + \text{CH}_2\text{I}^-$ Proton Transfer Reaction. *J. Phys. Chem. A* **2015**, *119*, 12517–12525.
- (39) Jiang, B.; Guo, H. Relative Efficacy of Vibrational vs. Translational Excitation in Promoting Atom-Diatom Reactivity: Rigorous Examination of Polanyi's Rules and Proposition of Sudden Vector Projection (SVP) Model. *J. Chem. Phys.* **2013**, *138*, 234104.
- (40) Stei, M.; Carrascosa, E.; Kainz, M. A.; Kelkar, A. H.; Meyer, J.; Szabó, I.; Czakó, G.; Wester, R. Influence of the Leaving Group on the Dynamics of a Gas-Phase $\text{S}_{\text{N}}2$ Reaction. *Nat. Chem.* **2016**, *8*, 151–156.
- (41) Szabó, I.; Olasz, B.; Czakó, G. Deciphering Front-Side Complex Formation in $\text{S}_{\text{N}}2$ Reactions via Dynamics Mapping. *J. Phys. Chem. Lett.* **2017**, *8*, 2917–2923.

(42) Szabó, I.; Császár, A. G.; Czakó, G. Dynamics of the $F^- + CH_3Cl \rightarrow Cl^- + CH_3F$ S_N2 Reaction on a Chemically Accurate Potential Energy Surface. *Chem. Sci.* **2013**, *4*, 4362–4370.

(43) Szabó, I.; Telekes, H.; Czakó, G. Accurate ab Initio Potential Energy Surface, Thermochemistry, and Dynamics of the $F^- + CH_3F$ S_N2 and Proton-Abstraction Reactions. *J. Chem. Phys.* **2015**, *142*, 244301.

(44) Liu, P.; Wang, D. Y.; Xu, Y. A New, Double-Inversion Mechanism of the $F^- + CH_3Cl$ S_N2 Reaction in Aqueous Solution. *Phys. Chem. Chem. Phys.* **2016**, *18*, 31895–31903.

(45) Liu, P.; Zhang, J.; Wang, D. Y. Multi-Level Quantum Mechanics Theories and Molecular Mechanics Study of the Double-Inversion Mechanism of the $F^- + CH_3I$ Reaction in Aqueous Solution. *Phys. Chem. Chem. Phys.* **2017**, *19*, 14358–14365.